Chem. Senses 36: 821–830, 2011

doi:10.1093/chemse/bjr057
Advance Access publication July 15, 2011

Structural Role of the Terminal Disulfide Bond in the Sweetness of Brazzein

Sannali M. Dittli[1], Hongyu Rao[2], Marco Tonelli[3], Jeniffer Quijada[4], John L. Markley[2,3], Marianna Max[5] and Fariba Assadi-Porter[2,3]

[1]Department of Chemistry, University of Wisconsin-Madison, 1101 University Drive, Madison, WI 53706, USA, [2]Biochemistry Department, University of Wisconsin-Madison, 433 Babcock Drive, Madison, WI 53706, USA, [3]National Magnetic Resonance Facility at Madison, University of Wisconsin-Madison, 433 Babcock Drive, Madison, WI 53706, USA, [4]Department of Pharmacology, New York University School of Medicine, 550 First Avenue, New York, NY 10016, USA and [5]Department of Neuroscience, Mount Sinai School of Medicine, 1 Gustave Levy Place, New York, NY 10029, USA

Correspondence to be sent to: Fariba Assadi-Porter, Biochemistry Department, University of Wisconsin-Madison, 433 Babcock Drive, Madison, WI 53706, USA. e-mail: fariba@nmrfam.wisc.edu

Accepted May 30, 2011

Abstract

Brazzein, a 54 residue sweet-tasting protein, is thought to participate in a multipoint binding interaction with the sweet taste receptor. Proposed sites for interaction with the receptor include 2 surface loops and the disulfide bond that connects the N- and C-termini. However, the importance of each site is not well understood. To characterize the structural role of the termini in the sweetness of brazzein, the position of the disulfide bond connecting the N- and C-termini was shifted by substituting K3-C4-K5 with C3-K4-R5. The apparent affinity and V_{max} of the C3-K4-R5-brazzein (CKR-brazzein) variant were only modestly decreased compared with the wild-type (WT) brazzein. We determined a high-resolution structure of CKR-brazzein by nuclear magnetic resonance spectroscopy (backbone root mean square deviation of 0.39 Å). Comparing the structure of CKR-brazzein with that of WT-brazzein revealed that the terminal β-strands of the variant display extended β-structure and increased dynamics relative to WT-brazzein. These results support previous mutagenesis studies and further suggest that, whereas interactions involving the termini are necessary for full function of brazzein, the termini do not constitute the primary site of interaction between brazzein and the sweet taste receptor.

Key words: brazzein, dynamics, multibinding site, sweet receptor, sweet-tasting protein

Introduction

The sweet taste receptor

The existence of a number of proteins with sweet-tasting (Morris and Cagan 1972; van der Wel 1972; Ming and Hellekant 1994; Nirasawa et al. 1994; Izawa et al. 1996; Masuda et al. 2001) or sweet taste modifying (Nakajima et al. 2006; Maehashi et al. 2007) properties poses one of the most interesting challenges in understanding sweet taste perception. Mammalian sweet taste perception is mediated by the Taste type 1 Receptor (T1R) family of class C G-Protein Coupled Receptors (GPCRs) (Nelson et al. 2001). Two subunits, T1R2 and T1R3, which have 48% sequence identity, form a heterodimeric receptor that recognizes all known sweet taste stimulants, from naturally occurring sugars and D-amino acids to various classes of artificial small molecule sweeteners to sweet-tasting proteins such as brazzein, thaumatin, monellin, and curculin (Li et al. 2002; Nelson et al. 2001, 2002; Suzuki et al. 2004; Nakajima et al. 2006). By analogy with the most closely related class C GPCR family, the metabotropic glutamate receptors, the T1R subunits are predicted to comprise 3 major domains: a large bilobed extracellular domain, the Venus Fly Trap Module (VFTM); a linker region containing 9 highly conserved cysteine residues, the Cysteine-Rich Domain (CRD); and the heptahelical transmembrane domain (Kitagawa et al. 2001; Max et al. 2001; Montmayeur et al. 2001; Sainz et al. 2001). By analogy to the solved crystal structure of the extracellular domain of metabotropic glutamate receptor 1 (Kunishima et al.

2000; Brock et al. 2007), the 2 lobes of the VFTMs of T1R2 and T1R3 are proposed to exist in a conformational equilibrium between an "open" state and a "closed" state. In the closed state, the lobes are closer together and the cleft between them forms a binding site for small molecule sweeteners such as sugars and dipeptides. Activation of the receptor is thought to involve closing of the VFTM of one or both subunits coupled to rotation of the subunits about their dimerization interface (Brock et al. 2007; Assadi-Porter, Maillet, et al. 2010). Binding of a small molecule ligand in the cleft of the closed VFTM subunit is thought to stabilize the activated form of the receptor. How the sweet proteins, which are orders of magnitude larger than the small molecule sweeteners and share no sequence or structural homology amongst them, activate the sweet taste receptor is not well understood.

Current theories favor a "wedge" model, wherein binding of sweet proteins occurs on a large surface overlapping the binding cleft of one receptor subunit (Temussi 2002; Spadaccini et al. 2003; Morini et al. 2005; Walters and Hellekant 2006), with additional contacts on the other subunit (Assadi-Porter, Maillet, et al. 2010), such that the conformational equilibrium of the receptor is shifted toward the activated form. Modeling efforts consistently dock the sweet proteins into cavities of the receptor surface that are complementary in charge and general shape to the surface of the sweet proteins themselves (Temussi 2002; Spadaccini et al. 2003; Morini et al. 2005; Walters and Hellekant 2006). A recent study (Assadi-Porter, Maillet, et al. 2010) of the sweet taste receptor found that mutations within the VFTM of T1R2 or T1R3 expected to interact with brazzein according to the "wedge" model failed to alter brazzein activity; instead, mutations within the CRD of T1R3 abolished brazzein activity. Although these results appear to disprove the previously proposed binding sites of wedge models, they suggest that the actual binding interaction between sweet proteins and the sweet taste receptor may be much more complex and subtle, probably involving multiple sites of interaction.

Brazzein

Brazzein, at 54 residues in length and ~6.4 kDa in mass, is the smallest and most extensively studied of the known sweet-tasting proteins (Ming and Hellekant 1994; Izawa et al. 1996; Caldwell et al. 1998; Assadi-Porter, Aceti, Cheng, et al. 2000; Assadi-Porter, Aceti, and Markley 2000; Assadi-Porter et al. 2003; Jin, Danilova, Assadi-Porter, Aceti, et al. 2003; Jin, Danilova, Assadi-Porter, Markley, et al. 2003; Assadi-Porter et al. 2008; Assadi-Porter, Malleti, et al. 2010; Assadi-Porter, Tonelli, et al. 2010). Brazzein is 19 000 times sweeter than sucrose on a per-molecule basis (Assadi-Porter et al. 2003). The solution structure of brazzein has been determined by nuclear magnetic resonance (NMR) spectroscopy (Caldwell et al. 1998). Brazzein folds into a 3-stranded antiparallel β-sheet and an α-helix according to Csβα fold family topology (Caldwell et al. 1998). It contains 8 cysteines, connected into a network of 4 disulfide bonds, resulting in a structure with a high degree of thermal and pH stability (Caldwell et al. 1998). Mutagenesis studies aimed at characterizing the sweetness-determining sites of brazzein have determined that the residues with the most profound effects cluster into 3 areas: the N- and C-termini, which are connected by a disulfide bond (site 1); the loop connecting the second and third strands of the β-sheet, denoted the R43 loop for the most critical residue in that group (site 2); and the partially structured loop connecting the first β-strand to the α-helical region of the protein, consisting of residues 9–19 (site 3) (Assadi-Porter, Aceti, Cheng, et al. 2000; Assadi-Porter, Aceti, Markley, et al. 2000; Assadi-Porter et al. 2003; Jin, Danilova, Assadi-Porter, Aceti, et al. 2003; Assadi-Porter, Tanelli, et al. 2010) (Figure 1). These sites are spatially distant from each other, yet on the same face of the protein, lending further support to a multipoint binding interaction model; however, the relative importance of the sites is not well understood.

Objectives of this research

We were intrigued by the unusual configuration of the C4–C52 disulfide bond in wild-type (WT) brazzein. The N- and C-termini of brazzein participate in an antiparallel β-sheet. Although in most cases, a disulfide bond between 2 strands of an antiparallel β-sheet is formed by cysteine residues found in directly opposing, nonhydrogen bonded positions of the strand registry (Wouters and Curmi 1995; Gunasekaran et al. 1997; Hutchinson et al. 1998), in brazzein, C4 and C52 occupy a diagonal arrangement, with C4 participating in hydrogen bonding with directly opposing residue Y51 (Figure 2A). The presence of an intact disulfide bond appears to be necessary for the sweet-tasting property of the protein; in a previous experiment (Assadi-Porter, Aceti, Cheng, et al. 2000), when C4 and C52 were simultaneously mutated to

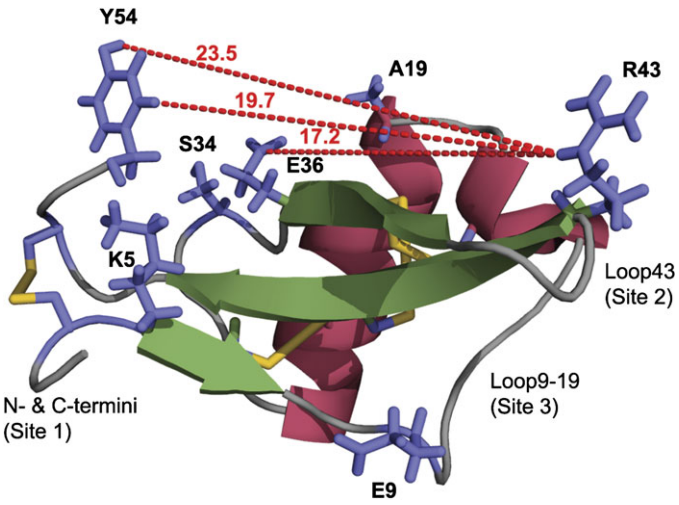

Figure 1 Solution structure of brazzein with sweetness-determining sites labeled. Side chains for sweetness-determining sites 1 and 2 are shown. Dashed lines indicate distances, in Ångstroms, between key residues of sites 1 and 2. This figure appears in color in the online version of *Chemical Senses*.

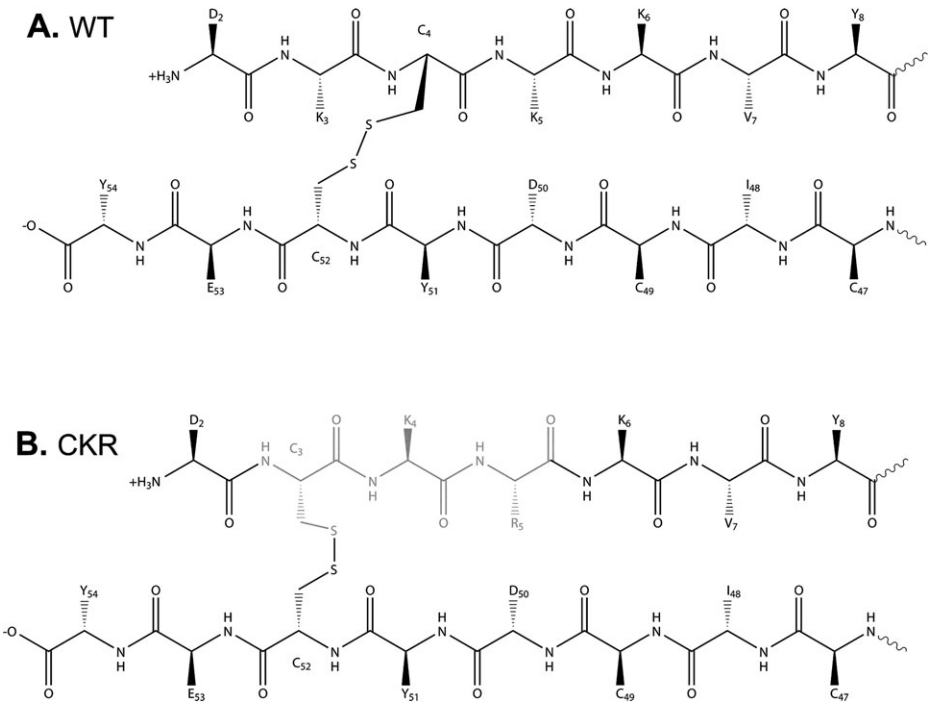

Figure 2 Sequence schematic of the β-sheet formed by the N- and C-termini of brazzein. **(A)** Sequence of WT-brazzein, showing hydrogen-bonding pattern and staggered conformation of terminal disulfide bond. **(B)** Sequence of CKR-brazzein, with changes from WT highlighted in gray, illustrating realignment of terminal disulfide bond.

alanine (A4,A52-brazzein), thus removing the terminal disulfide bond, the variant exhibited a 4-fold loss of sweetness (Assadi-Porter, Aceti, Cheng, et al. 2000; Assadi-Porter, Aceti, Markley, et al. 2000; Assadi-Porter, Maillet, et al. 2010). We sought to determine whether the role of the terminal disulfide bond in brazzein was merely to enforce spatial proximity of the termini or if the unusual configuration of that disulfide bond also contributed to the sweetness of brazzein.

The rationale for switching residues K3 and C4 was to allow the terminal disulfide bond to form across directly opposing, nonhydrogen bonded positions of the β-strand registry. This change created a run of 3 consecutive lysine residues, K4–K6, in the N-terminal strand. Recognizing that this feature of the primary sequence would lead to overlap and ambiguity in the NMR spectra, we made a conservative substitution at position 5 from the WT lysine (K) to arginine (R). We prepared the K5R single mutant (K5R-brazzein) to verify our assumption that this conservative mutation would be structurally and functionally neutral. We then made a double mutant of the K5R construct resulting in the K3C/C4K/K5R triple mutant (Figure 2B), which is hereafter referred to as CKR-brazzein.

Experimental procedures

Expression and purification

WT- and CKR-brazzein samples were overproduced in *Escherichia coli* by using the SUMO fusion system according to previously reported protocols (Assadi-Porter et al. 2008). K5R-brazzein samples were overproduced in *E. coli* using a staphylococcal nuclease fusion, as previously described (Assadi-Porter, Maillet, et al. 2010). Reverse-phase-HPLC (RP-HPLC) column chromatography was used as the final brazzein purification step and for assessment of sample purity. Tris-Tricine (16%) gel chromatography was used to assay the extent of SUMO-protease proteolysis activity and recovery of brazzein product. Folding of the protein was checked by RP-HPLC and by NMR (Assadi-Porter et al. 2008).

NMR data collection

NMR samples were prepared by dissolving 2–3 mg of lyophilized protein in 10% D_2O and adjusting the pH to 5.2, the same value used for WT-brazzein (Caldwell et al. 1998). Spectra were collected at 37 °C on Varian Unity-Inova 600 and 800 MHz spectrometers equipped with *z* axis gradient cold probes. Resonances from backbone atoms were assigned by analyzing ^{15}N-HSQC, CBCA(CO)NH, HNCACB, and HNCO spectra. Data from C(CO)NH, HC(CO)NH, HBHA(CO)NH, and ^{13}C-HSQC spectra were used in assigning resonances from side chain atoms. Manual resonance assignments were confirmed and areas that were difficult to assign manually were assigned automatically with PINE-NMR software (Bahrami et al. 2009). Nuclear Overhauser effect (NOE) distance restraints for the structure calculations were obtained from isotope-edited NOESY spectra (^{15}N- and ^{13}C-HSQC-NOESY). Hydrogen

bonds identified from 2D HNCO data collected with a delay time (66.5 ms) optimized for detection of long-range ^{15}N–$^{13}C'$ scalar couplings (*trans*-H-bond couplings) (Cordier and Grzesiek 1999; Assadi-Porter et al. 2003). Spectra were processed with nmrPipe (Delaglio et al. 1995) and analyzed with SPARKY (Goddard and Kneller 2000) software. NMR data for CKR-brazzein were deposited at BMRB with entry accession #16978, and atom coordinates were deposited at PDB (ID: 2YQ and RCSB101740).

Structure calculations

CYANA 3.0 (Herrmann et al. 2002; Güntert 2004) was used for structure calculations with partially assigned NOE peak lists (short range and unambiguous long-range NOEs, described below) and φ and ψ angle predictions obtained from TALOS (Cornilescu et al. 1999) as initial restraints. Sequential H_i^N to H_i^α and/or H_{i-1}^α NOEs and NOEs associated with cysteine H^β resonances were assigned; all other NOEs were picked, but left unassigned. A limited selection of hydrogen bonds identified as those that were both predicted by CYANA from the preliminary structure calculations and observed in the long-range HNCO spectrum were used as additional restraints for a further round of calculations. Alignments were performed and structures were rendered for display in PyMol (DeLano 2002).

Dynamics studies

Heteronuclear Overhauser effect (HetNOE) (Kay et al. 1989) data were collected via a modified ^{15}N-HSQC pulse sequence with and without a 3 s ^1H saturation delay time (Kay et al. 1989) on a 600 MHz Varian NMR spectrometer.

Heterologous calcium assay for sweet taste receptor

HEK293E cells were cultured at 37 °C in Optimum GlutaMAX culture medium (Invitrogen) supplemented with 4% dialyzed fetal bovine serum. Human T1R2 and T1R3 receptor clones were constructed as described previously (Jiang et al. 2004). The $G_{\alpha16}$-gust44 construct was made according to Ueda et al. (2003). Cells were transfected using Lipofectamine 2000 according to the manufacturer's protocol (Invitrogen). Cells were seeded onto 96-well poly-D-lysine plates (Corning) at about 12 500 cells/well 18 h prior to transfection; cells in each well were cotransfected with plasmid DNAs encoding T1Rs and $G_{\alpha16}$-gust44 (0.1 μg total DNA/well; 0.2 μL Lipofectamine/well). After 24 h, the transfected cells were washed once with the culture medium. After an additional 24 h, the cells were washed once with Hank's balanced salt solution (HBSS), loaded with 3 μM Fluo-4AM (Molecular Probe) diluted in HBSS buffer, incubated for 1.5 h at room temperature, and then washed with HBSS and maintained in HBSS at 25 °C. The plates of dye-loaded transfected cells were placed into a FlexStation II apparatus (Molecular Devices) to monitor fluorescence (excitation, 488 nm; emission, 525 nm; cutoff, 515 nm). Tastants were added 30 s after the start of the scan at a range of concentrations in 50 μL of HBSS while monitoring fluorescence for an additional 200 s at 2 s intervals (Assadi-Porter, Tonelli, et al. 2010).

Analysis of calcium responses

After obtaining a calcium mobilization trace for each sample, the calcium response to each tastant was quantified as the change in signal from baseline (peak fluorescence) after subtracting buffer control (denoted as ΔF) and noted by arbitrary fluorescent units. Peak fluorescence intensity occurred about 20–30 s after the addition of tastants. Tastants evoked no significant responses from parental cells. The data were expressed as the mean ± standard error of quadruplicate or sextuplicate of the ΔF values. The data analysis and curve-fitting routines were carried out using GraphPad Prism 3.0 (GraphPad Software, Inc.).

Results

Structure of CKR-brazzein

The ^{15}N-HSQC spectra of CKR-brazzein and K5R-brazzein were well dispersed in both the ^1H and the ^{15}N dimensions, indicating that the proteins are stably folded. The changes in the ^{15}N-HSQC peak positions of K5R-brazzein relative to those of WT-brazzein are shown mapped onto the structure of WT-brazzein in Figure 3A. The most significant chemical shift differences were at the point of mutation (residue 5) and at a nearby residue Y54. The changes in the ^{15}N-HSQC peak positions of CKR-brazzein relative to those of WT-brazzein are shown mapped onto the structure of WT-brazzein in Figure 3B. Most resonances of CKR-brazzein overlapped or were close to corresponding resonances of WT-brazzein, except in areas surrounding the mutated N-terminal sequence. The chemical shift differences between K5R-brazzein and CKR-brazzein are similar to those between WT-brazzein and CKR-brazzein (Figure 3C). These data show that the structural differences between CKR-brazzein and WT-brazzein primarily arise from the switching of K3 and C4 to realign the terminal disulfide bond.

The residues exhibiting the largest differences in ^{15}N-HSQC peak positions between WT-brazzein and CKR-brazzein were residues 3–6 of the N-terminal β-strand and residues C49–E53 of the C-terminal β-strand, as expected due to the proximity of these residues to the altered disulfide bond (Figure 3B,C). Large changes in the position of ^{15}N-HSQC peaks were also observed for residues R33–E36. These residues, located in the loop between the end of the α-helix and the third β-strand, which packs closely against the terminal disulfide, are in the near vicinity of the termini. The changes in these residues suggest that the conformation of the termini has changed fairly significantly, leading to an altered packing of the nearby loop.

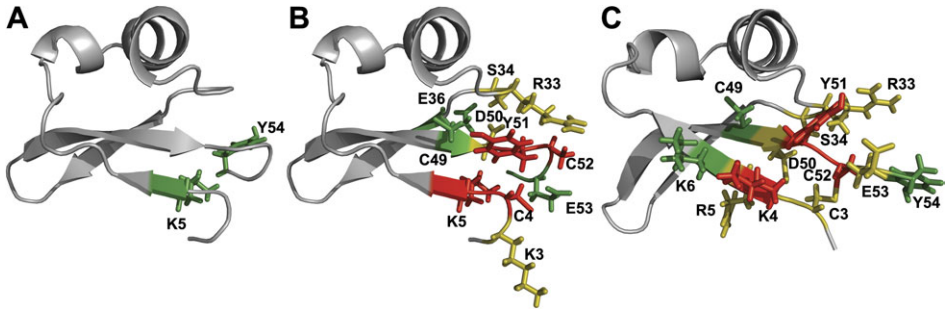

Figure 3 Chemical shift differences between the ^{15}N-HSQC spectra of WT-brazzein, K5R-brazzein, and CKR-brazzein mapped onto the structure of brazzein (Caldwell et al. 1998). Red indicates a difference of >|5| ppm in ^{15}N or |0.5–1| ppm in ^{1}H; yellow indicates a difference of |2–5| ppm in ^{15}N or |0.2–0.5| ppm in ^{1}H; green indicates a difference of |1–2| ppm in ^{15}N or |0.1–0.2| ppm in ^{1}H; residues are colored according to the dimension which displayed the most extreme difference. Residues colored light gray changed by <|1| ppm in ^{15}N and <|0.1| ppm in ^{1}H. **(A)** Differences between WT-brazzein and K5R-brazzein mapped onto the structure of WT-brazzein. **(B)** Differences between WT-brazzein and CKR-brazzein mapped onto the structure of WT-brazzein. **(C)** Differences between K5R-brazzein and CKR-brazzein mapped onto the structure of CKR-brazzein.

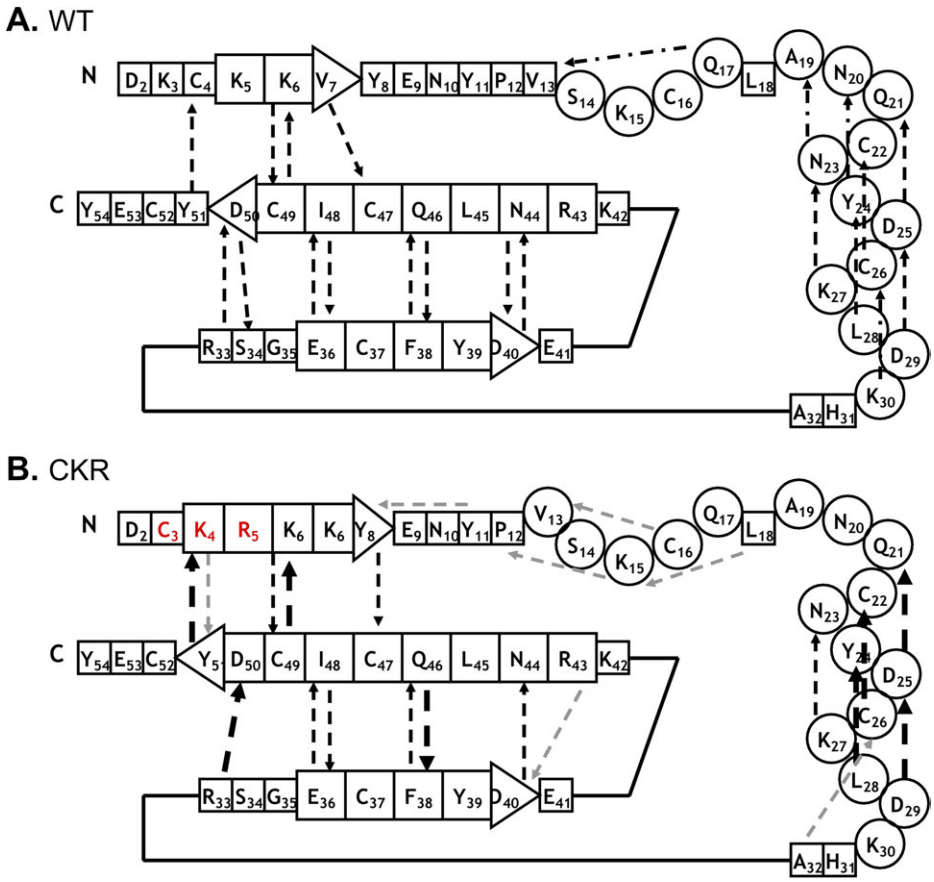

Figure 4 Schematic representation of hydrogen bonding in CKR-brazzein. Small squares, large squares or triangles, and circles indicate regions of random coil, β-sheet, and α-helix, respectively. Dashed arrows indicate hydrogen bonds, pointing from amide hydrogen to carbonyl oxygen. **(A)** Hydrogen-bonding pattern of WT-brazzein. Adapted from Assadi-Porter et al. (2003). **(B)** Hydrogen-bonding pattern of CKR-brazzein. Bolded arrows were experimentally observed in both CKR-brazzein and WT-brazzein (Assadi-Porter et al. 2003); nonbolded arrows were identified by CYANA in CKR-brazzein and experimentally observed in WT-brazzein (Assadi-Porter et al. 2003); gray arrows were identified by CYANA in CKR-brazzein but not experimentally observed in either CKR-brazzein or WT-brazzein.

Eight hydrogen bonds (bolded arrows in Figure 4) were unambiguously identified in the long-range HNCO spectrum of CKR-brazzein, in contrast to the 17 bonds observed for WT-brazzein (Assadi-Porter et al. 2003). Twelve additional hydrogen bonds were identified by CYANA in the structural ensemble but not observed by *trans*-H-bond coupling.

Hydrogen bonds, observed in WT-brazzein but not in CKR-brazzein, are located along one face of the α-helix and between the second and third β-strands. Two key hydrogen bonds for maintaining sweetness (Assadi-Porter et al. 2003), one between the amide hydrogen of K27 and the carbonyl oxygen of N23 and the other between the amide hydrogen of E36 and the carbonyl oxygen of I48, were not observed by *trans*-H-bond coupling but were identified as present in the structures generated by CYANA. A third diagnostic hydrogen bond, between the amide hydrogen of Y51 and the carbonyl oxygen of K4, was observed, albeit with very weak intensity, in the long-range HNCO spectrum. The hydrogen-bonding pattern of the termini of WT-brazzein is only partially preserved in CKR-brazzein.

Although resonance overlap prevented some of the expected cross-disulfide NOEs from being observed, the $^{13}C^{\beta}$ chemical shifts of all cysteine residues in CKR-brazzein were consistent with formation of all 4 disulfide bonds, including the one between the termini (Table 1) (Wishart and Nip 1998).

The ensemble of 20 structures of CKR-brazzein had a backbone atom RMSD of 0.39 ± 0.09 Å and heavy atom RMSD of 1.17 ± 0.13 Å and aligned with the structure of WT-brazzein with an RMSD of 3.21 Å (Figure 5A). Overall the structures of CKR-brazzein and WT-brazzein were very similar; however, a number of significant differences existed. As expected given the consecutive triple mutation of the primary sequence of the N-terminal strand, multiple differences were observed for the N- and C-termini. In WT-brazzein, an NOE between the H^{α} atoms of D50 and Y54 indicated that the termini are folded back upon themselves (Caldwell et al. 1998; Assadi-Porter et al. 2003); however, in CKR-brazzein, this NOE was not observed, and the termini displayed a fully extended structure. The straightening of the termini accounted for the dramatic chemical shift change observed for the ^{15}N-HSQC peak of residue S34 because this residue was no longer within the sphere of influence of the phenyl ring of the Y54 side chain (Figure 5B). The 3–10 helix was extended by one residue, beginning at V13 in CKR-brazzein versus S14 in WT-brazzein. The region of β-type structure in the N-terminal strand extends from residue K5 to residue V7 in WT-brazzein (βI); in CKR-brazzein, the region of β-type structure in the N-terminal strand was lengthened and extended from residue K4 to residue Y8. The C-terminal β-strand (βII) was also lengthened by one residue, extending

Table 1 Chemical shifts of cysteine $^{1}H^{\alpha}$ and $^{13}C^{\beta}$ atoms in CKR-brazzein

Residue	δ Hα	δ Cβ
Ref, reduced	*4.55*	*28.0*
Ref, oxidized	4.71	41.1
CKR, C3	5.43	46.5
CKR, C16	4.74	40.6
CKR, C22	*4.31*	38.8
CKR, C26	*4.11*	36.7
CKR, C37	6.13	46.1
CKR, C47	4.82	38.4
CKR, C49	5.37	37.0
CKR, C52	5.16	46.3

Values corresponding to a reduced state are italicized for easier identification. Reference chemical shift values are taken from Wishart and Nip (1998).

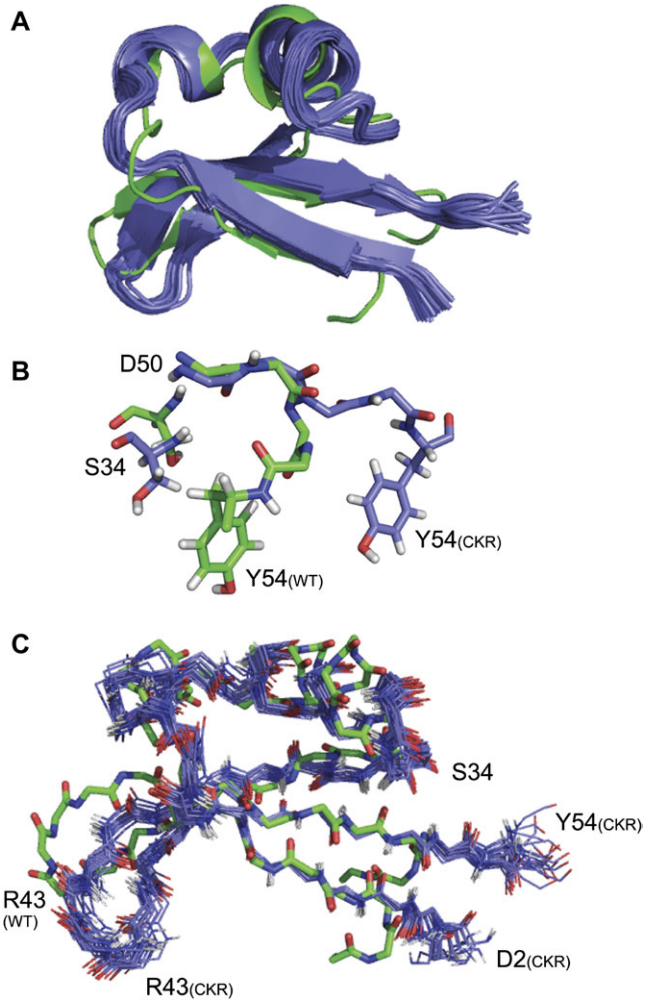

Figure 5 Alignment of WT-brazzein (green) and CKR-brazzein (blue). **(A)** Global alignment of WT-brazzein with the ensemble of CKR-brazzein structures, RMSD 3.21 Å. The CKR-brazzein bundle had a backbone atom RMSD of 0.39 ± 0.09 Å and heavy atom RMSD of 1.17 ± 0.13 Å. **(B)** Spatial relationship of S34 and Y54 in WT-brazzein and CKR-brazzein. The C-termini of WT-brazzein and CKR-brazzein are shown as backbone starting from D50. Residues S34 and Y54 are shown in their entirety. In WT-brazzein, the α-protons of S34 and Y54 are separated by ~10 Å, whereas in CKR-brazzein, the distance between the α-protons of S34 and Y54 is ~15 Å. **(C)** Pairwise alignment of K4–Y8 and C47–Y51 of CKR-brazzein with corresponding residues of WT-brazzein, RMSD 0.78 Å. Structures were aligned by matching the carbonyl oxygen of each residue of CKR-brazzein with the carbonyl oxygen of the corresponding residue of WT-brazzein. Side chains are omitted for clarity.

to Y51 in CKR-brazzein where it ends at D50 in WT-brazzein. The third β-strand, extending from E36 to D40 (βIII), was unchanged in length.

Residues K4–Y8 and C47–Y51 of CKR-brazzein, corresponding to the β-strands, were aligned with the respective residues of WT-brazzein; the average pairwise RMSD for aligning the ensemble of 20 CKR-brazzein structures with WT-brazzein was 0.78 Å. Although the backbone atoms of residues K4–Y8 and C47–Y51 aligned well, showing that, aside from the straightening of the termini, the conformation of the terminal β-strands was relatively unchanged, aligning the terminal β-strands exaggerated the changes in the conformation of loop regions in the protein (Figure 5C). Loop43 (sweetness-determining site 2) appears to be bent closer to the solvent-exposed face of the β-sheet, but the distance between Loop43 and the termini is increased significantly. In WT-brazzein, the distance between R43 and Y54 is approximately 20 Å (see Figure 1), whereas in CKR-brazzein the same distance is approximately 30 Å. The α-helix appears to pack against the β-sheet more closely as well. The β-sheet of CKR-brazzein appears to be more twisted than the β-sheet of WT-brazzein, likely in consequence of the reduced distance between the N-terminal β-strand and Loop9–19 (sweetness-determining site 3) and of the bending of Loop43 toward the solvent-exposed β-sheet face.

Dynamics of CKR-brazzein

The HetNOE values determined for WT-brazzein and CKR-brazzein are very similar (Figure 6). CKR-brazzein appears to be significantly more flexible at each end of Loop9–19 (site 3). This increase in flexibility may offset steric strains induced by the lengthening of the N-terminal β-strand and 3–10 helix.

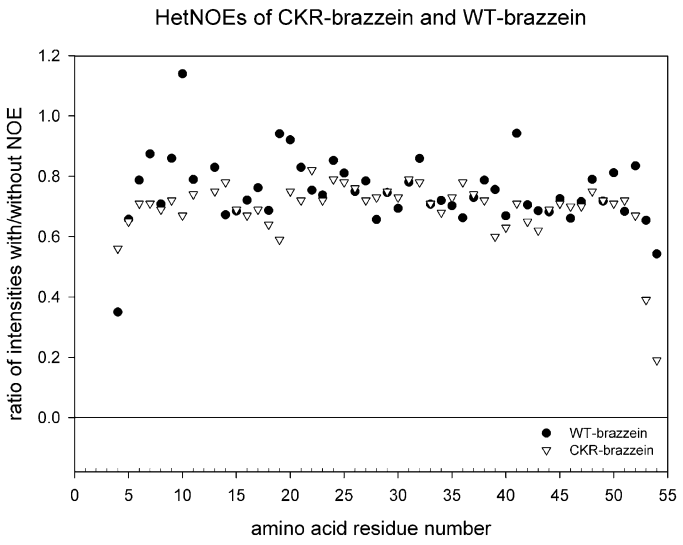

Figure 6 Internal dynamics of CKR-brazzein relative to WT-brazzein. Higher HetNOE values indicate structural rigidity and lower values indicate structural flexibility on a pico- to nanosecond timescale. Excepting the termini, the largest differences were observed for residues N10, A19, and E41. Loop43 and in particular residue E41 are also strikingly more flexible in CKR-brazzein, consistent with the structural flexing of Loop43 (site 2) toward the β-sheet. The moderate increase in flexibility at D50 is consistent with loss of the hydrogen bond between D50 and S34 (see Figure 4). The structure of the C-terminus of CKR-brazzein displays a more extended structure than that of WT-brazzein, consistent with the Het-NOE values indicating that it is considerably more flexible.

Biological activity of CKR-brazzein

We performed concentration–response experiments to determine the effect of the CKR mutations on activity using heterologous expression of the sweet receptor and a calcium mobilization assay (see Experimental procedures). The concentration–response (Figure 7) showed a modest reduction in the apparent affinity of the variant compared with WT (EC50 8.9 μM and 16.7 μM for WT and CKR, respectively). The CKR variant also showed a modest reduction in maximal response (12 205 for WT-brazzein vs. 9771 for CKR-brazzein). The moderate reduction in sweetness caused by realigning the terminal disulfide bond suggests that the structural restraint of an intact disulfide bond at the termini

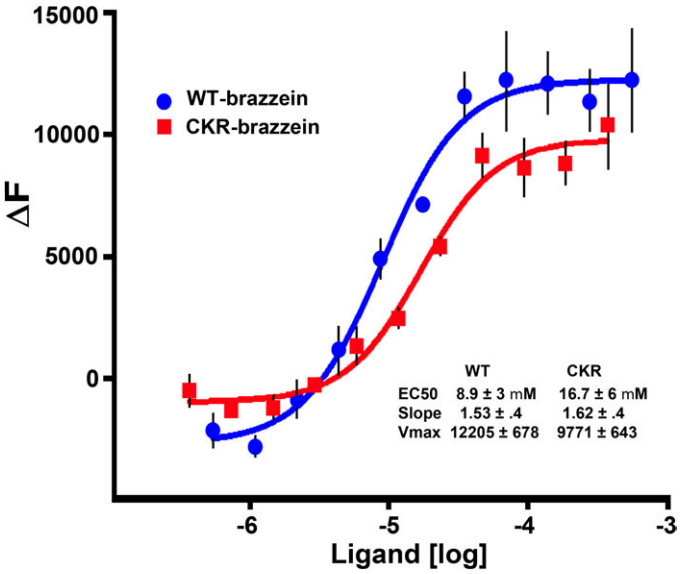

Figure 7 Activity differences between WT-brazzein and CKR-brazzein. Concentrations of each brazzein variant were added to cultures of HEK293E cells which had been previously transfected with sweet receptor and G-protein reporter G-protein constructs (T1R2, T1R3, and $G_{\alpha 16}$-gust44). Responses were monitored with a fluorescent calcium mobilization assay (see Experimental procedures) and plotted to show concentration dependent responses. WT-brazzein responses (circles) and CKR-brazzein (squares) were each used to calculate a response curve. The CKR variant had a modestly right shifted apparent affinity compared with WT-brazzein (8.9 and 16.7 mM) but reached saturation at nearly the same activity level as WT-brazzein. The modest change in affinity and potency results in ~25–40% reduction in apparent sweetness over the linear range of responses. The data were expressed in arbitrary fluorescent units as the mean ± standard error of quadruplicate or sextuplicate of the Δ*F*. This figure appears in color in the online version of *Chemical Senses*.

contributes to the high activity of brazzein; a 4-fold reduction in sweetness was previously observed when the terminal disulfide bond was removed entirely by mutating both C4 and C52 to alanine (A4,A52-brazzein) (Assadi-Porter, Aceti, Cheng, et al. 2000; Assadi-Porter, Aceti, Markely, et al. 2000; Assadi-Porter, Maillet. et al. 2010).

Discussion

A previous experiment in which the terminal disulfide bond of brazzein was abolished by the double mutation C4A,C52A demonstrated that the presence of an intact disulfide bond at the termini is necessary for the intense sweetness of the protein (Assadi-Porter, Aceti, Cheng, et al. 2000; Assadi-Porter, Aceti, Markley, et al. 2000; Assadi-Porter, Maillet, et al. 2010). Our present results indicate that in addition to the presence of the terminal disulfide bond, its unusual native configuration must also be preserved for brazzein to exhibit full activity. The principal difference between WT-brazzein and CKR-brazzein is the realignment of the native diagonal disulfide to a straightened disulfide by switching the positions of residues K3 and C4. The contribution of the K5R mutation to CKR-brazzein phenotype appears to be essentially neutral because K5R-brazzein displayed nearly identical ^{15}N-HSQC chemical shifts to WT-brazzein (Figure 3A) and had comparable sweetness (Assadi-Porter, Maillet, et al. 2010). The changes in the structure and modest reduction in sweetness of CKR-brazzein can therefore be attributed primarily to the change in the configuration of the terminal disulfide bond and its relative distance to the other distant proposed sweet sites (Loop43 and Loop19), suggesting that the sweetness may be maintained by the other distant sites.

Although the side chain functional groups at the termini of CKR-brazzein are primarily preserved between WT- and CKR-brazzein, the spatial presentation of these groups is dramatically altered. The backbone β-structure of the termini is strengthened in CKR-brazzein compared with WT, but the hydrogen-bonding pattern is weakened, a change typically associated with greatly reduced sweetness (Assadi-Porter et al. 2003). Despite these changes, CKR-brazzein appears to have lost only a modest amount of its sweetness. The altered structure and hydrogen-bonding pattern of the CKR variant reduces apparent affinity only minimally while also reducing potency by ~20% which reduces sweetness over the linear range by <50%. Our previous work suggests that the initial interaction between brazzein and the sweet taste receptor occurs at D535 of the T1R3 CRD, which when mutated to glutamine abolishes all binding and activity (Assadi-Porter, Tonelli, et al. 2010). Given the modest effect of the CKR mutations on activity despite major local structural changes at the termini, it seems unlikely that this region is involved in binding at the critical T1R3 CRD receptor binding site. The reduced maximal responses that are specific to brazzein are also observed when several residues of the VFTM of T1R2 are mutated (Maillet, Quijada and Max, unpublished data) and when mouse T1R2 VFTM sequence replaces that of human (Assadi-Porter, Maillet, et al. 2010), suggesting that this region is a plausible site of interaction with secondary binding and activation by brazzein.

Previous experiments demonstrated that mutation of D50 to alanine (near the C-terminus and in sweetness-determining site 1) also led to changes of hydrogen-bonding pattern and internal dynamics in Loop43 (sweetness-determining site 2) (Assadi-Porter, Aceti, Cheng, et al. 2000; Assadi-Porter, Aceti, Markley, et al. 2000; Assadi-Porter, Maillet, et al. 2010). Likewise, mutations in Loop43 were accompanied by changes in the hydrogen-bonding pattern and internal dynamics of the termini (Assadi-Porter et al. 2003). The mutations in the N-terminal strand of CKR-brazzein led not only to changes in the structure and dynamics of the termini, as expected, but also to structural and dynamic changes in the distant Loop43 and the nearby Loop9–19 (sweetness-determining site 3) and Loop34 sites. The termini and Loop43 sweetness-determining sites thus appear to be closely coupled, perhaps with Loop9–19 acting as the hinge by which conformational information is transmitted between the other 2 sites. In CKR-brazzein, the R43 loop became more flexible, and its spatial relationship to other parts of the protein was altered; most notably, the distance between residue R43 and residue Y54 was increased by approximately 10 Å. The contribution of these changes in Loop43 to the reduced sweetness of CKR-brazzein is not easily deconvoluted from those of the changes at the termini; however, the observation that the sweetness of CKR-brazzein is similar to that of WT-brazzein indicates that the 2 proteins have similar interactions with the sweet taste receptor despite the large structural changes at the termini. Combined with previous mutagenesis results (sweetness order WT-brazzein = K5R-brazzein > CKR-brazzein > A4,A52-brazzein) (Assadi-Porter, Aceti, Cheng, et al. 2000; Assadi-Porter, Aceti, Markley, et al. 2000; Assadi-Porter, Maillet, et al. 2010), these data suggest that, whereas the type and orientation of side chains at the termini of brazzein are important for function, a site other than the termini may be the primary site of interaction with the receptor while other sites serve to stabilize its active structure. Further structural studies of sweeter and nonsweet mutations in the distant proposed sweet sites in Loop43 and Loop19 are underway to examine their structures and their possible contributions to the termini.

Conclusion

The diagonal disulfide bond at the termini of WT-brazzein is unusual in that disulfide bonds in native protein β-sheet structures are most frequently found in opposing registry positions (Wouters and Curmi 1995; Gunasekaran et al. 1997; Hutchinson et al. 1998). Changing the configuration of the terminal disulfide bond in CKR-brazzein led to a 10 Å increase in the distance between the termini and Loop43

sweetness-determining sites, greatly increased the flexibility of the termini, and moderately reduced the sweetness of the variant. These results demonstrate that the nonstandard diagonal disulfide bond configuration found in WT-brazzein plays a key role in brazzein's rare property of intense sweetness and suggest that it may restrict the conformational space accessible to the termini such that the distance between the 2 sites most closely matches the optimal partner sites on the sweet taste receptor in a multipoint binding interaction.

Funding

This research was supported by the National Institutes of Health [R01 DC009018 and R21 DC008805 to F.A.P., R01 DC006696 and R01 DC008301 to M.M, and P41 RR02301 which funds the National Magnetic Resonance Facility at Madison].

References

Assadi-Porter FM, Abildgaard F, Blad H, Markley JL. 2003. Correlation of the sweetness of variants of the protein brazzein with patterns of hydrogen bonds detected by NMR spectroscopy. J Biol Chem. 278: 31331–31339.

Assadi-Porter FM, Aceti DJ, Cheng H, Markley JL. 2000. Efficient production of recombinant brazzein, a small, heat-stable sweet-tasting protein of plant origin. Arch Biochem Biophys. 376:252–258.

Assadi-Porter FM, Aceti DJ, Markley JL. 2000. Sweetness determinant sites of brazzein, a small, heat-stable, sweet-tasting protein. Arch Biochem Biophys. 376:259–265.

Assadi-Porter FM, Maillet EL, Radek JT, Quijada J, Markley JL, Max M. 2010. Key amino acid residues involved in multi-point binding interactions between brazzein, a sweet protein, and the T1R2-T1R3 human sweet receptor. J Mol Biol. 398:584–599.

Assadi-Porter FM, Patry S, Markley JL. 2008. Efficient and rapid protein expression and purification of small high disulfide containing sweet protein brazzein in E. coli. Protein Expr Purif. 58:263–268.

Assadi-Porter FM, Tonelli M, Maillet EL, Markley JL, Max M. 2010. Interactions between the human sweet-sensing T1R2-T1R3 receptor and sweeteners detected by saturation transfer difference NMR spectroscopy. Biochim Biophys Acta. 1798:82–86.

Bahrami A, Assadi A, Markley JL, Eghbalnia H. 2009. Probabalistic interaction network of evidence algorithm and its application to complete labeling of peak lists from protein NMR spectroscopy. PLoS Comput Biol. 5(3):e1000307.

Brock C, Ouselati N, Soler S, Boudier L, Rondard P, Pin JP. 2007. Activation of a dimeric metabotropic glutamate receptor by intersubunit rearrangement. J Biol Chem. 282:33000–33008.

Caldwell JE, Abildgaard F, Dzakula Z, Ming D, Hellekant G, Markley JL. 1998. Solution structure of the thermostable sweet-tasting protein brazzein. Nat Struct Biol. 5:427–431.

Cordier F, Grzesiek S. 1999. Direct observation of hydrogen bonds in proteins by interresidue $^{3h}J_{NC'}$ scalar couplings. J Am Chem Soc. 121: 1601–1602.

Cornilescu G, Delaglio F, Bax A. 1999. Protein backbone angle restraints from searching a database for chemical shift and sequence homology. J Biomol NMR. 13:289–302.

Delaglio F, Grzesiek S, Vuister GW, Zu G, Pfiefer J, Bax A. 1995. NMRPipe: a multidimensional spectral processing system based on UNIX pipes. J Biomol NMR. 6:277–293.

DeLano WL. 2002. The PyMol molecular graphics system. San Carlos (CA): DeLano Scientific LLC Available from: http://www.pymol.org.

Goddard TD, Kneller DG. 2000. SPARKY 3. San Francisco (CA): University of California.

Güntert P. 2004. Automated NMR structure calculation with CYANA. Methods Mol Biol. 278:353–378.

Gunasekaran K, Ramakrishnan C, Balaram P. 1997. β-Hairpins in proteins revisited: lessons for *de novo* design. Protein Eng. 10:1131–1141.

Herrmann T, Güntert P, Wütrich K. 2002. Protein NMR structure determination with automated NOE assignments using the new software CANDID and the torsion angle dynamics algorithm DYANA. J Mol Biol. 319:209–227.

Hutchinson EG, Sessions RB, Thornton JM, Woolfson DN. 1998. Determinants of strand register in antiparallel beta-sheets of proteins. Protein Sci. 7:2287–2300.

Izawa H, Ota M, Kohmura M, Ariyoshi Y. 1996. Synthesis and characterization of the sweet protein brazzein. Biopolymers. 39:95–101.

Jiang P, Ji Q, Liu Z, Snyder LA, Benard LM, Margolskee RF, Max M. 2004. The cysteine-rich region of T1R3 determines responses to intensely sweet proteins. J Biol Chem. 279:45068–45075.

Jin Z, Danilova V, Assadi-Porter FM, Aceti DJ, Markley JL, Hellekant G. 2003. Critical regions for the sweetness of brazzein. FEBS Lett. 544:33–37.

Jin Z, Danilova V, Assadi-Porter FM, Markley JL, Hellekant G. 2003. Electrophysiological and human psychophysical responses to mutants of the sweet protein brazzein: delineating brazzein sweetness. Chem Senses. 28:491–498.

Kay LE, Torchia DA, Bax A. 1989. Backbone dynamics of proteins as studied by ^{15}N inverse detected heteronuclear NMR spectroscopy: application to staphylococcal nuclease. Biochemistry. 28:8972–8979.

Kitagawa M, Kusakabe Y, Miura H, Ninomiya Y, Hino A. 2001. Molecular genetic identification of a candidate receptor gene for sweet taste. Biochem Biophys Res Commun. 283:236–242.

Kunishima N, Shimada Y, Tsuji Y, Sato T, Yamamoto M, Kumasaka T, Nakanishi S, Jingami H, Morikawa K. 2000. Structural basis of glutamate recognition by a dimeric metabotropic glutamate receptor. Nature. 407: 971–977.

Li X, Staszewski L, Xu H, Durick K, Zoller M, Adler E. 2002. Human receptors for sweet and umami taste. Proc Natl Acad Sci U S A. 99: 4692–4696.

Maehashi K, Matano M, Kondo A, Yamamoto Y, Udaka S. 2007. Riboflavin-binding protein exhibits selective sweet suppression toward protein sweeteners. Chem Senses. 32:183–190.

Masuda T, Ueno Y, Kitabatake N. 2001. Sweetness and enzymatic activity of lysozyme. J Agric Food Chem. 49:4937–4941.

Max M, Shanker YG, Huang L, Rong M, Liu Z, Campagne F, Weinstein H, Damak S, Margolskee RF. 2001. *Tas1r3*, encoding a new candidate taste receptor, is allelic to the sweet responsiveness locus *Sac*. Nat Genet. 28: 58–63.

Ming D, Hellekant G. 1994. Brazzein, a new high-potency thermostable sweet protein from Pentadiplandra brazzeana B. FEBS Lett. 355: 106–108.

Montmayeur JP, Liberles SD, Matsunami H, Buck LB. 2001. A candidate taste receptor gene near a sweet taste locus. Nat Neurosci. 4:492–498.

Morini G, Bassoli A, Temussi PA. 2005. From small sweeteners to sweet proteins: anatomy of the binding sites of the human T1R2_T1R3 receptor. J Med Chem. 48:5520–5529.

Morris JA, Cagan RH. 1972. Purification of monellin, the sweet principle of Dioscoreophyllum cumminsii. Biochim Biophys Acta. 261:114–122.

Nakajima K, Asakura T, Oike H, Morita Y, Shimizu-Ibuka A, Misaka T, Sorimachi H, Arai S, Abe K. 2006. Neoculin, a taste-modifying protein, is recognized by human sweet taste receptor. Neuroreport. 17:1241–1244.

Nelson G, Chandrashekar J, Hoon MA, Feng L, Zhao G, Ryba NJP, Zucker CS. 2002. An amino-acid taste receptor. Nature. 416:199–202.

Nelson G, Hoon MA, Chandrashekar J, Zhang Y, Ryba JP, Zucker CS. 2001. Mammalian sweet taste receptors. Cell. 106:381–390.

Nirasawa S, Nishino T, Katahira M, Uesugi S, Hu Z, Kurihara Y. 1994. Structures of heat-stable and unstable homologues of the sweet protein mabinlin. Eur J Biochem. 223:989–995.

Sainz E, Korley JN, Battey JF, Sullivan SL. 2001. Identification of a novel member of the T1R family of putative taste receptors. J Neurochem. 77: 896–903.

Spadaccini R, Trabucco F, Saviano G, Picone D, Crescenzi O, Tancredi T, Temussi PA. 2003. The mechanism of interaction of sweet proteins with the T1R2-T1R3 receptor: evidence from the solution structure of G16A-MNEI. J Mol Biol. 328:683–692.

Suzuki M, Kurimoto E, Nirasawa S, Masuda Y, Hari K, Kurihara Y, Shimba N, Kawai M, Suzuki E, Kato K. 2004. Recombinant curculin heterodimer exhibits taste-modifying and sweet-tasting activites. FEBS Lett. 573: 135–138.

Temussi PA. 2002. Why are sweet proteins sweet? Interaction of brazzein, monellin and thaumatin with the T1R2-T1R3 receptor. FEBS Lett. 526: 1–4.

Ueda T, Ugawa S, Yamamura H, Imaisumi Y, Shimada S. 2003. Functional interaction between T2R taste receptors and G-protein alpha subunits expressed in taste receptor cells. J Neurosci. 23:7376–7380.

van der Wel H. 1972. Isolation and characterization of the sweet principle from Dioscoreophyllum cumminsii (Stapf) Diels. FEBS Lett. 21: 88–90.

Walters DE, Hellekant G. 2006. Interactions of the sweet protein brazzein with the sweet taste receptor. J Agric Food Chem. 54: 10129–10133.

Wishart DS, Nip AM. 1998. Protein chemical shift analysis: a practical guide. Biochem Cell Biol. 76:153–163.

Wouters MA, Curmi PMG. 1995. An analysis of side chain interactions and pair correlations within antiparallel β-sheets: the differences between backbone hydrogen-bonded and non-hydrogen bonded residue pairs. Proteins. 22:119–131.